

# A Novel Force Sensing Integrated into the Trocar for Minimally Invasive Robotic Surgery

G. A. Fontanelli, L. R. Buonocore, F. Ficuciello, L. Villani, B. Siciliano

**Abstract**—Minimally invasive robotic surgery holds a fundamental role in modern surgery. However, one of its major limitations compared to classic laparoscopy is that the surgeon can only rely on visual perception, for the lack of haptic force feedback. A new solution for a force sensor placed at the end-tip of the trocar is presented here. This solution allows measuring the interaction forces between the surgical instrument and the environment without any changes to the instrument structure and with full adaptability to different robot platforms and surgical tools. A prototype of the sensor has been realized with 3D printed technology for a proof of concept. The static and dynamic characterization of the sensor is provided together with experimental validation.

## I. INTRODUCTION

Minimally Invasive Robotic Surgery (MIRS) has revolutionized surgical and therapeutic procedures by changing their effect on patients and significantly reducing collateral damages. In MIRS, to perform surgery or deliver therapy, the instruments enter the patients body through one or more small incisions. With respect to the classical open surgery, this procedure leads to improved outcomes, reduced recovery time, decreased hospitalization, and improved cosmesis.

One of the major limitations of these robot-aided procedures is the lack of haptic force feedback for the surgeon. This represents an important challenge for the community of robotic surgery researchers. As a matter of fact, the loss of tactile and kinesthetic information leads to several limitations:

- Tissues palpation, for structures identification or properties/texture assessment, is no longer allowed.
- Large forces, that lead to trauma and damage of healthy tissues, could be accidentally applied.
- During re-constructive surgical procedures, the surgeons do not have any feedback of the applied forces on the suturing thread or on the tissues. Consequently, the suturing thread may be broken and tissues damaged.
- It is impossible to identify undesired interactions between the instruments and the environment (organs) outside the viewing area.

On the other hand, studies on this topic [1] found out that haptic feedback reduces unintentional injuries during dissection tasks and reduces learning time for novices.

Several works on the development of force sensing to measure the interaction between surgical instruments and the patient body, based on different kind of technologies, are

The authors are with the Interdepartmental Center for Advances in Robotic Surgery of the University of Naples Federico II. Corresponding author's email: giuseppeandrea.fontanelli@unina.it

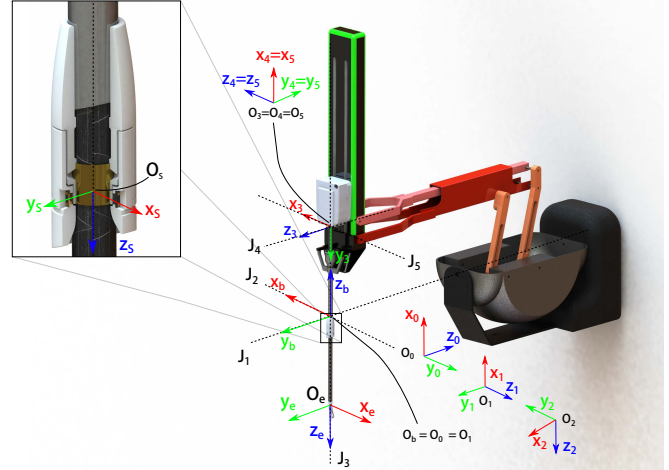


Fig. 1. The da Vinci PSM robotic arm with the force sensor in the trocar.

available in the literature. Some of them investigate the possibility to provide force measurement without making changes to the robot, e.g. in [2] using only visual information or, as in [3] and [4], using the robot joint torques measurements.

On the other hand, many prototypes of sensorized surgical instruments have been developed by integrating force sensors in the instrument shaft or wrist, or even in the gripper fingers and clamp faces. In [5], strain gauges are mounted on an aluminum frame and attached upstream the instrument wrist. This allows to measure all forces and torques acting on the instrument end-effector. Bragg reticula are used in [6] to realize a 6 DOF sensor. The Bragg technology has many advantages, including the immunity to the EMI noise and the high integration capability. A simple solution, relying on Bragg technology to measure the forces on the plane orthogonal to the shaft of the surgical instrument, is presented in [7]. Optical solutions like that used in [8] to develop a sensitive skin could be adapted for sensing the forces directly on the surgical gripper, as well as solutions based on piezoelectric effect, as those evaluated in [9] and [10].

The common feature of all the above works is that they require the modification of the instrument structure to integrate the force sensor. This entails higher costs, problems related to the sterilization, greater likelihood of instrument breakage, the need of miniaturized complex structures able to withstand high stresses.

In this work, a novel solution for sensing the interaction force between the robot tools and the patient body is evaluated. The proposed sensing device is capable of measuring the forces in the orthogonal plane of the surgical

instruments. As a matter of fact, these two force components can be poorly reconstructed using model-based estimation algorithms, because of friction and tendon elasticity of the surgical tools that are difficult to model and identify [11].

The main idea is to place the sensor in the trocar with minimal modification of its structure and without modifying the surgical instruments. A similar, but more complex solution can be found in [12], in which an adapter for the da Vinci robot is developed using the overcoat method in order to measure the three components of force. As far as we know, this is the first solution proposed in the literature, based on the measure of the interaction forces between the trocar and the instrument sliding inside. This allows to avoid surgical tool modifications, thus reducing costs and expenditure of time. Moreover, it has full adaptability to different robot platforms and surgical tools.

## II. SENSOR TECHNOLOGY AND OPERATING PRINCIPLE

In this section, the structure, technology and electronics of the sensor are described together with the main mechanical properties and performance. The innovation consists on conceiving the structure, hosting the sensor element, to be allocated at the end-tip of the trocar. This serves for the estimation of the interaction forces between the instrument end-effector and the patient body, by measuring the forces generated by the displacement of the instrument shaft with respect to the fixed trocar pipe. The sensing device allows measuring the forces placed on the orthogonal plane of the surgical instruments. Fig. 1 shows a rendering of the da Vinci Patient Side Manipulator (PSM) with a zoomed view of the trocar where the sensor is placed. A sensor reference frame  $O_s-x_s y_s z_s$  attached to the sensor is defined, with the axes  $x_s$  and  $y_s$  lying on a plane orthogonal to the trocar axis. More details about the inherent operating principle are provided below.

A little gap between the instrument shaft and the trocar exists to guarantee the reciprocal sliding. When the forces are exerted on the instrument's end-effector, the component acting along  $x_s$  and  $y_s$  causes a misalignment (eccentricity) between the instrument and the trocar axes. This leads to contacts between the trocar, where the sensor is placed, and the instrument. In those contact points the forces are discharged causing deformation of the elastic frames that compose the sensor.

The main idea is to measure the eccentricity between the instrument shaft and the fixed trocar using four proximity optical sensors mounted in appropriate way. This eccentricity is proportional to the force components acting in the plane orthogonal to the instrument axis and depends on the elasticity of the deformable frames. This solution have some advantages with respect to the state of the art:

- 1) No modifications of the robotic laparoscopic instruments are needed. This allows containing the costs and preserving the instrument properties. Indeed, the modification of the surgical instrument may cause a

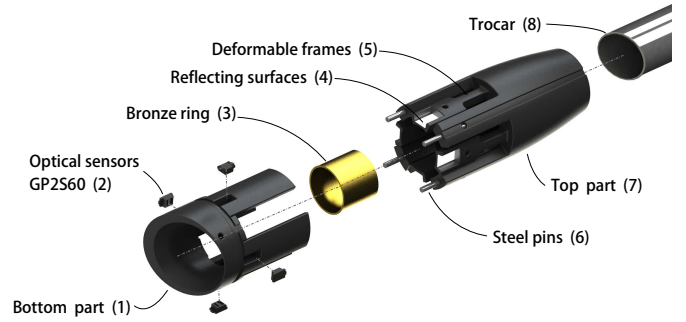


Fig. 2. Exploded view of the force sensor mechanical structure.

structural weakening due to the dimensions of the shaft that usually has a diameter between 5 and 10 mm.

- 2) The forces measured by a sensor attached to the trocar are not influenced by the tendon driven mechanism forces, as happens for the sensors allocated at the instrument shaft [7].
- 3) Compared to solutions with sensors located at the end-tip of the instruments, the connection cables and the data acquisition system are fixed and far away from the surgical site.
- 4) Last but not least, the sensor (structure and acquisition system) is cheap and could be disposable.

In the next subsections, the mechanical structure, the optical sensors and the electronic systems for signals acquisition and processing are described.

### A. Mechanical structure

The sensor is designed to be added, as a tube extension, at the end of the standard trocar used in laparoscopic robotic systems. Fig. 2 shows the exploded view of the finite model of the sensor. The sensor is composed by three main parts. With reference to Fig. 2, the top part (7) is attached at the end-tip of the trocar and is constituted by four deformable frames designed with four digs holding flat reflective surfaces; the surgical instrument slides inside a bronze ring (3) that is glued on the four deformable frames in order to ensure a homogeneous deformation; in correspondence of the reflective surfaces, four optical sensors are fixed to the bottom part of the sensor (1).

In this first prototype, the parts have been produced in plastic using a 3D printed technology based on the polyjet process. This technology was chosen due to the high precision and quick fabrication time, without difficult cleaning procedure or post print treatment. However, as highlighted in Sec. IV, this technology is not suitable to realize the final version of the sensor because the mechanical properties of the printed material are not stable and change with time.

### B. FEM analysis

A Finite Element Model-based (FEM-based) optimization procedure was used to define the optimal dimensions of the deformable frames according to the following specifications:

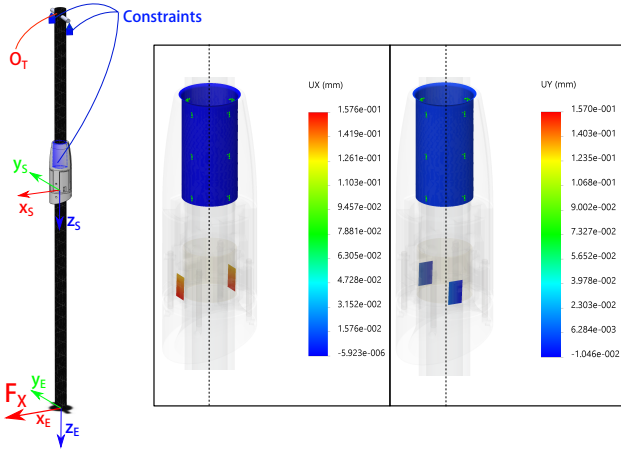


Fig. 3. FEM analysis of the sensor prototype: (left) CAD model; (middle) displacement along axis  $x_S$ ; (right) displacement along  $y_S$  axis.

- The force range along  $x_S$  and  $y_S$  axes is chosen in the range  $[-20, 20]$  N.
- The maximum of the von Mises stress (safety factor) is settled as two times the value of the material yield stress that is in the range  $[50, 65]$  MPa.
- The minimum size of the structure has to meet the constraints of the printer.
- Minimization of the overall diameter of the structure is desired.

A FEM analysis was carried out on a prototype designed according to the above specifications, to validate the expectation of the project pre-requirements. The behavior of the sensor was simulated when a force  $F_x = 10$  N is applied to the instrument end-effector along the  $x_E$  axis of a frame  $O_E-x_Ey_Ez_E$  attached to the instrument's tip. The connection point  $O_T$  between the tool shaft and the box on the top of the tool, represented in Fig. 3, was considered as stuck. In the same way, the end-tip of the trocar was considered as a fixed point since it constitutes a constraint for the motion of the tool shaft except for the sliding motion (see the image on the left of Fig. 3).

In the configuration considered in the FEM simulation, the tool is displaced in the trocar in such a way that the end-effector frame has a distance from the  $O_T$  point that is two times the distance of the sensor frame from the same point. Hence, due to the lever mechanism, a force of 20 N results applied along the  $x_S$ -axis of the sensor frame.

In Fig. 3 the displacement of the four reflective surfaces is shown. First of all, the analysis shows a stress effect on the deformable structure about two times lower than the yield stress value, that for the used material is around  $7e7$  N/m<sup>2</sup>. Furthermore, it is possible to observe that a force applied along the  $x_S$ -axis causes a displacement of the reflecting surfaces (the two in orange) perpendicular to the  $x_S$ -axis while the other two surfaces (in blue) move parallel to themselves. Thus, a force exerted along the  $x_S$ -axis has no effect on the deformable components placed on the  $y_S$ -axis and the deformations of the structure caused by the forces along the  $x_S$  and  $y_S$  are decoupled as desired.

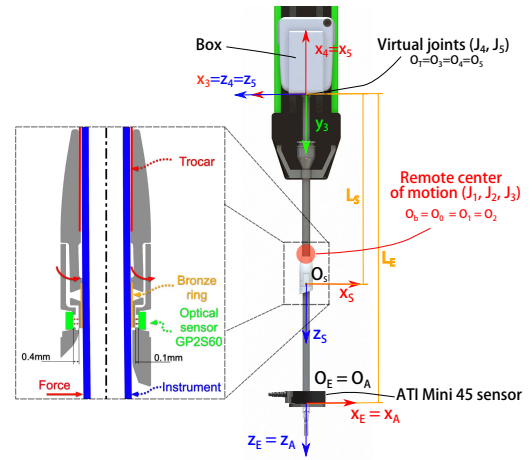


Fig. 4. Front view of the instrument and of the sensor.

The eccentricity between the instrument shaft and the fixed trocar caused by a force exerted along the  $x_S$ -axis is highlighted in the zoomed area of Fig. 4. The interaction force between the instrument end-effector and the environment causes a displacement of the instrument tool that collides with the trocar, and thus with the bronze ring of the trocar sensor glued to the four deformable frames. The displacements of the frames reported in the figure corresponds to a force of 20 N.

### C. Optical sensor

This first prototype of the sensor was realized using *GP2S60* optical sensors to measure the deformation of the structure. The optical sensors are positioned in suitable trays purposely designed. Each sensor measures the distance between itself and the little plate in front of it. With reference to Fig. 5, the working area of the prototype sensor is the region in the interval  $[0 - 0.4]$  mm where the characteristic is linear and the electrical gain is very high.

The sensor is equipped with an IR source and a photodiode detector capable of measuring the amount of reflected light, so that the distance between the sensor and a reflective surface in front of it is measured. This kind of sensor is affected by light interference and cross-talk disturbance. To reduce these effects, all the external parts of the sensor are painted in black, excepted for the reflective surfaces which are painted in white. The polarization circuit is dimensioned so that output voltage signal can move from  $-2$  V to  $2$  V for a displacement of  $\pm 0.2$  mm.

To improve the sensibility of the sensor, two optical devices are located on the same axes but in the opposite directions. Thus, for a movement of the sensible structure, one sensor will detect a positive displacement while the other one will detect a negative displacement. The differential reading allows increasing the gain two times. A software calibration procedure is implemented to delete the residual bias that is not compensated by the differential acquisition system.

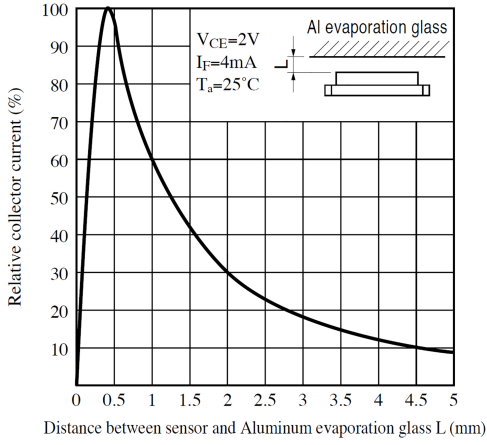


Fig. 5. GP2S60 optical sensor characteristic curve.

#### D. Electronics

Even though the proximity IR light sensor is not affected by electromagnetic interference (EMI), a little acquisition system to limit the interference is mounted very close to the sensor. This device was selected to comply with space limitations while preserving the possibility of a differential reading and signal pre-amplification. The *ADS1015* analog to digital converter (ADC) was selected for the application since it is equipped with four channel AD converter and allows the differential reading mode.

Four proximity sensors, located at 90 deg one from another, are read in a differential way to increase the resolution. The chosen ADC has the possibility to set an internal amplifier. To maximize the resolution in the measure range, the amplification factor was set to *EIGHT*. Finally, the converter device is equipped with a serial bus I2C to minimize the number of connection wires, reduced to four, which allows a simplified connection of the sensor.

A mbed platform [13] (the microcontroller *LPC1768*) was selected for signal acquisition and numerical pre-filtering. The maximum frame rate of the ADC in the differential acquisition mode is 1.5 KHz, and the signals are filtered at frequency of 1 KHz. The system is able to acquire the signal with a 12 bit resolution, which is good enough for this application.

### III. SENSOR CHARACTERIZATION

The sensor has been tested on the da Vinci Patient Side Manipulator (PSM), represented in Fig. 1.

The PSM is a 7-DOF actuated arm, which moves the attached instrument with respect to a Remote Center of Motion (RCM), i.e., a mechanically-fixed point that is invariant with respect to the configuration of the PSM joints. The first 6 degrees of freedom correspond to Revolute (R) and Prismatic (P) joints, in a RRP RR sequence. The joint axes are shown in Fig. 1, where are denoted as  $J_i, i = 1, \dots, 3$ . The position of the instrument's tip depends only on the first 3 joint variables, collected in the vector  $\mathbf{q} = [\theta_1, \theta_2, d_3]^T$ . The last 4 joints allow the opening/closure and reorientation of the gripper mounted on the tip.

The sensor is mounted in the terminal part of the trocar, which is placed in the RCM point and can rotate with the instrument about the axes  $J_1$  and  $J_2$  intersecting in the RCM. The instrument can also translate with respect to the trocar and the sensor along the axis  $J_3$ .

The  $(2 \times 1)$  vector  $\mathbf{f}_S$  of the forces applied to the sensor are related to the  $(3 \times 1)$  vector  $\mathbf{f}_E$  of the forces applied to the end-effector at the instrument tip. This relationship depends on the distance of the end-effector from the trocar but also on the gravity forces acting on the instrument and, in the presence of motion, also on instrument's shaft inertia. These latter effects are neglected in a first analysis.

#### A. Static analysis

Assuming static conditions and absence of gravity, we consider two virtual joints in the  $O_T$  point,  $J_4$  and  $J_5$  represented in Fig. 4, where the shaft (a carbon fiber tube), considered rigid, is connected to the box of the instrument. The relationship between  $\mathbf{f}_S$  and  $\mathbf{f}_E$  can be simply obtained from the static equilibrium of the forces, as follows:

$$\begin{cases} \boldsymbol{\tau}_G = \mathbf{J}_E^T \mathbf{f}_E \\ \boldsymbol{\tau}_G = \mathbf{J}_S^T(\mathbf{q}) \mathbf{f}_S \end{cases} \implies \mathbf{f}_E = (\mathbf{J}_E^T)^\dagger \mathbf{J}_S^T(\mathbf{q}) \mathbf{f}_S, \quad (1)$$

where  $\boldsymbol{\tau}_G$  is the  $(2 \times 1)$  torque vector at the two virtual joints, and the Jacobian matrices  $\mathbf{J}_E$  and  $\mathbf{J}_S$  can be computed as:

$$\mathbf{J}_E = \begin{bmatrix} L_E & 0 \\ 0 & L_E \\ 0 & 0 \end{bmatrix} \quad \mathbf{J}_S(\mathbf{q}) = \begin{bmatrix} L_S & 0 \\ 0 & L_S \end{bmatrix} \quad (2)$$

being  $L_S = (0.43 - q_3)$ ,  $L_E = 0.389$  and  $q_3 = d_3$  the prismatic joint variable of the PSM.

Notice that the third element of vector  $\mathbf{f}_E$  computed in (1) is always null, because the sensor allows to measure only the components of the interaction force lying in the plane orthogonal to the instrument's shaft, corresponding to the first two elements of  $\mathbf{f}_E$ .

#### B. Sensor calibration

The sensor is able to measure the voltage that is proportional to the eccentricity of the bronze ring with respect to the axis of the sensor. This eccentricity is produced by the forces applied to the ring along the axis  $x_S$  and  $y_S$  and depends on the elasticity of the deformable frames, assumed to be linear. The calibration of the sensor is aimed at computing the calibration matrix  $\mathbf{W}$  mapping the vector of the sensed voltages  $\mathbf{v}_S$  to the measured forces  $\mathbf{f}_S$ , i.e.,

$$\mathbf{f}_S = \mathbf{W} \mathbf{v}_S.$$

To this purpose, a commercial force-torque sensor *ATI Mini 45* was linked to the instrument end-effector using a 3D structure printed on purpose, with the axes  $(x_A, y_A, z_A)$  of the ATI reference frame aligned to the axes  $(x_E, y_E, z_E)$  of the end-effector frame (see Fig. 4).

The calibration is performed by applying manually a force on the ATI sensor and reading the signals of the two sensors

simultaneously. The ATI sensed forces are mapped to the trocar sensor frame using the equation

$$\mathbf{f}_A^S = \mathbf{J}_S(\mathbf{q})^{-T} \mathbf{J}_E^T \mathbf{f}_A$$

obtained by inverting the mapping in (1). The numerical value of the calibration matrix was then derived as

$$\mathbf{W} = \mathbf{F}_A^S \mathbf{V}_S^\dagger,$$

being  $\mathbf{F}_A^S$  and  $\mathbf{V}_S$  the matrices obtained by stacking the measurements of  $\mathbf{f}_A^S$  and  $\mathbf{v}_S$  respectively. The resulting value is:

$$\mathbf{W} = \begin{bmatrix} 35.7188 & -5.8590 \\ 0.2335 & 33.7922 \end{bmatrix}.$$

### C. Dynamic analysis

Because of the position of the sensor, attached to the end-tip of the trocar, the measure is influenced by the gravity and inertial forces due to the mass and inertia of the instrument's shaft. This implies that the sensor measurements can be different from zero also in the absence of interaction. If a CAD model of the instrument is available, these effects could be computed on line and compensated.

In this paper, a model of the gravity and inertia effects is derived and compared with the sensor readings in the absence of interaction. In detail, the torques on the two virtual joints  $J_4$  and  $J_5$  intersecting at the point  $O_T$  of the instrument, due to gravity and inertia, are computed from the force  $\mathbf{f}_S$  measured by the sensor as

$$\boldsymbol{\tau}_M = \mathbf{J}_S^T(\mathbf{q}) \mathbf{f}_S. \quad (3)$$

The same torques can be obtained through the symbolic computation of the Lagrangian dynamic model of the instrument, with the following assumptions (see Fig. 4):

- The instrument can rotate with respect to the remote center of motion RCM about the axes  $J_1$  and  $J_2$ , with joint variables  $q_1$  and  $q_2$  respectively.
- The instrument can translate along the axis  $J_3$ , with joint variables  $q_3$ .
- The two virtual joints  $J_4$  and  $J_5$  have zero velocities and accelerations.

Only the torques on the last two virtual joints are of interest, that can be written in the form

$$\boldsymbol{\tau}_I = \begin{bmatrix} b_1 \ddot{q}_1 + g_1 \\ b_2 \ddot{q}_2 + g_2 \end{bmatrix} \quad (4)$$

with:

$$g_1 = 9.81 m p_x \sin(q_1)$$

$$g_2 = 9.81 m p_x \cos(q_1) \sin(q_2)$$

$$b_1 = m p_x \cos(q_2) (q_3 - L_R) - I_{yy} \cos(q_2)$$

$$b_2 = m p_x (q_3 - L_R) - I_{zz}$$

were the variable  $L_R$  represents the distance between the point  $O_T$  and the RCM when  $q_3 = 0$ . Notice that for simplicity the instrument has been modeled as a cylinder and the Coriolis and centrifugal terms have been neglected.

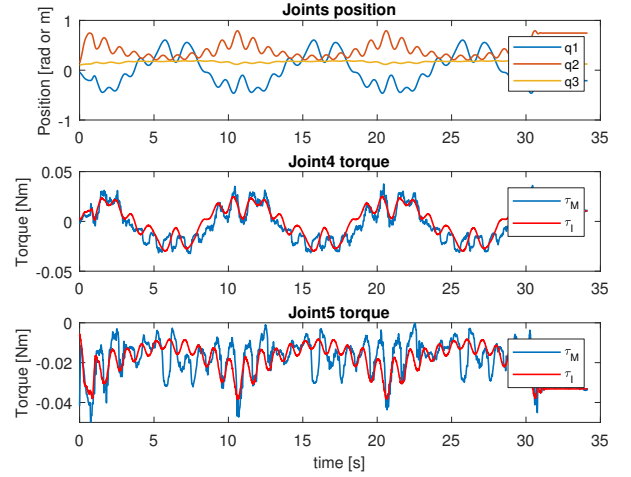


Fig. 6. Comparison of the torques  $\tau_I$  computed using the dynamic model with the torques  $\tau_M$  computed using the sensor measurements. The corresponding time histories of the joint variables are reported in the top of the figure.

In Fig. 6, the torques  $\tau_M$  computed in (3) using the sensor measurements and the torques  $\tau_I$  computed in (4) using the sensor readings of the first 3 joints of the PSM are shown. The following numerical values of the dynamic parameters, derived from a CAD model of the instrument (a needle driver gripper), have been used:

$$\beta = \begin{bmatrix} m p_x \\ I_{yy} \\ I_{zz} \end{bmatrix} = \begin{bmatrix} -5.1e^{-3} \\ 8e^{-4} \\ 8e^{-4} \end{bmatrix}$$

The time histories of the joint variables are reported in the top of the figure. It is possible to observe that the torques computed using the dynamic model are quite close to the measured ones.

Notice that, for the case of the instrument used in the experiments, the dynamic effects are small compared to the range of the measured forces (about 1% of the maximum force) and could be neglected. Of course, when instruments with higher weight and inertia are used, the dynamic effects should be compensated.

## IV. EXPERIMENTAL VALIDATION

The validation of the sensor and of the static model is performed applying a force to the ATI sensor while the surgical instrument is in motion along the  $J_3$  axis as shown in Fig. 7 (bottom). The force measured by the ATI sensor, the force measured by the trocar sensor reported in the end-effector frame using the equation 1, and the relative error are shown in Fig. 7.

The results show that the sensor has a good response close to that of the commercial sensor ATI mini 45. The error between the ATI sensor and the trocar sensor is less than 12% for both the axis. The error is higher in the central region of the graph, when a constant force is applied to the sensor. This is due to the properties of the material used for the prototype. In polyjet technology for additive manufacturing (AM), the printed materials are composted layer by layer. Thus, the mechanical properties are not homogeneous like

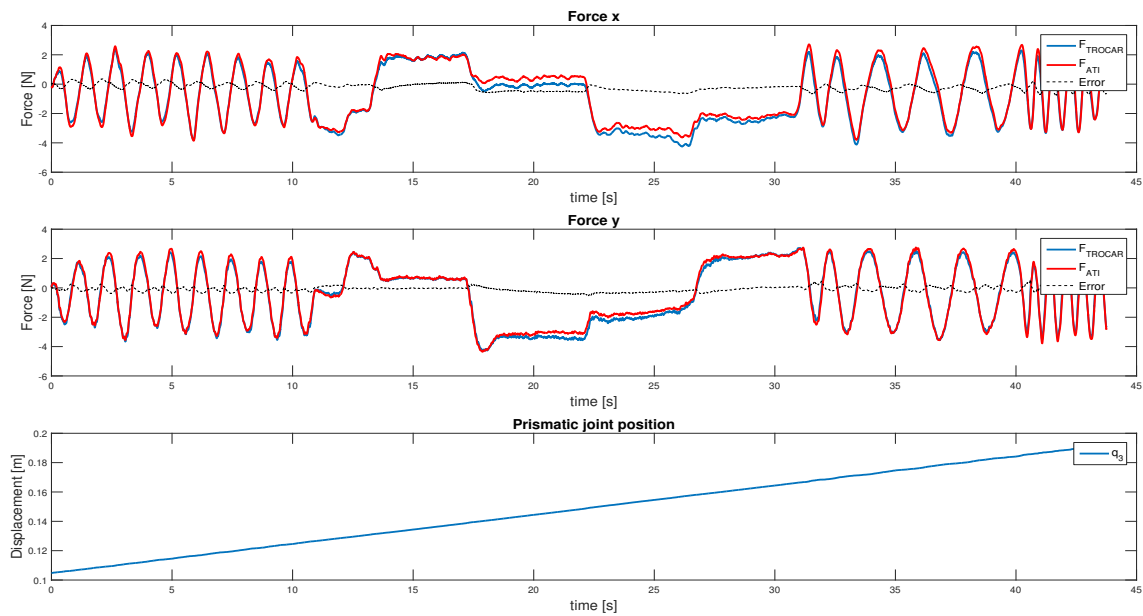


Fig. 7. Static characterization: force along the axis  $x_E$  (top), force along the axis  $y_E$  (middle) and prismatic joint trajectory (bottom).

for standard bulk material, and the products presents a certain degree of anisotropy, a viscoelastic behavior and hysteresis [14]. Moreover, the elastic properties of the printed prototype change as a function of the time and of the applied force amplitude.

## V. CONCLUSION AND FUTURE WORKS

In this work a new concept of force sensing for MIRS is evaluated. The proposed solution differs from the previous force sensors presented in the literature since it does not require the modification of the surgical instruments, exploiting the possibility of placing the sensor in the trocar. This opens the way for new disposable, low cost and simple force sensors that can be universal with respect to the chosen tool, allowing force feedback on different set-up, even on clinical robotic surgical systems currently used in operating rooms. The prototype presented in the paper was printed using polyjet 3D printing technology only for proof of concept. In future works a prototype suitable to be used in a real surgical scenario will be developed. In particular, with respect to the first prototype, this sensor should be made of a reliable material with good response to stresses and stable behavior with respect to the time. Finally, new algorithms for hybrid force reconstruction will be analyzed to extend the range of measure and to integrate also the measurement of the force along the axis  $z$ .

## VI. ACKNOWLEDGMENT

This research has been partially funded by the EC Seventh Framework Programme (FP7) within RoDyMan project 320992 and by the national grant MURHAR under Programma STAR linea 1.

## REFERENCES

[1] T. Ortmaier, B. Deml, G. Passig, D. Reintsema, and U. Seibold, "Robot Assisted Force Feedback Surgery," *Advances in Telerobotics*, vol. 31, pp. 361–379, 2007.

[2] A. Petit, F. Ficuciello, G. A. Fontanelli, L. Villani, and B. Siciliano, "Using Physical Modeling and RGB-D Registration for Contact Force Sensing on Deformable Objects," in *IEEE International Conference on Informatics in Control, Automation and Robotics*, 2017.

[3] F. Ficuciello, L. Villani, and B. Siciliano, "Variable impedance control of redundant manipulators for intuitive human-robot physical interaction," *IEEE Transactions on Robotics*, vol. 31, pp. 850–863, 2015.

[4] —, "Impedance control of redundant manipulators for safe human-robot collaboration," *Acta Polytechnica Hungarica, Journal of Applied Science, Special Issue on Recent Advances in Robotics*, vol. 13, pp. 223–238, 2016.

[5] U. Seibold, B. Kubler, and G. Hirzinger, "Prototype of instrument for minimally invasive surgery with 6-axis force sensing capability," in *IEEE International Conference on Robotics and Automation*, 2005, pp. 496–501.

[6] R. Haslinger, P. Leyendecker, and U. Seibold, "A fiberoptic force-torque-sensor for minimally invasive robotic surgery," in *IEEE International Conference on Robotics and Automation (ICRA)*, 2013, pp. 4390–4395.

[7] R. Xu, A. Escoto, K. S. Shahzada, C. Ward2, and R. V. Patel, "A method for installing fbg sensors inside surgical robotic instruments," in *The Hamlyn Symposium on Medical Robotics*, 2016.

[8] A. Cirillo, F. Ficuciello, C. Natale, S. Pirozzi, L. Villani, and B. Siciliano, "A conformable force/tactile skin for physical human-robot interaction," *IEEE Robotics and Automation Letters*, vol. 1, pp. 41–48, 2015.

[9] U. Kim, D. H. Lee, H. Moon, J. C. Koo, and H. R. Choi, "Design and realization of grasper-integrated force sensor for minimally invasive robotic surgery," in *IEEE/RSJ International Conference on Intelligent Robots and Systems*, 2014, pp. 4321–4326.

[10] M. O. Culjat, C. H. King, M. L. Franco, C. E. Lewis, J. W. Bisley, E. P. Dutton, and W. S. Grundfest, "A tactile feedback system for robotic surgery," in *IEEE International Conference of the Engineering in Medicine and Biology Society*, 2008, pp. 1930–1934.

[11] G. A. Fontanelli, F. Ficuciello, L. Villani, and B. Siciliano, "Modelling and identification of the da Vinci research kit robotic arms," in *IEEE/RSJ International Conference on Intelligent Robots and Systems*, 2017.

[12] S. Shimachi, S. Hirunyanitwatna, Y. Fujiwara, A. Hashimoto, and Y. Hakozaki, "Adapter for contact force sensing of the da vinci robot," in *International Journal of Medical Robotics and Computer Assisted Surgery*, vol. 4, 2008, pp. 121–130.

[13] mbed: Development Platform for Devices. [Online]. Available: <https://developer.mbed.org/platforms/mbed-LPC1768/>

[14] D. Blanco, P. Fernandez, and A. Noriega, "Nonisotropic experimental characterization of the relaxation modulus for polyjet manufactured parts," *Journal of Materials Research*, 2014.